Published in final edited form as:
Dev Biol. 2006 March 1; 291(1): 83–95. doi:10.1016/j.ydbio.2005.12.021.

Differential expression of espin isoforms during epithelial morphogenesis, stereociliogenesis and postnatal maturation in the developing inner ear

Gabriella Sekerková, **Lili Zheng**, **Enrico Mugnaini**, and **James R. Bartles**
Department of Cell and Molecular Biology, Feinberg School of Medicine, and Institute for Neuroscience, Northwestern University, Chicago, IL 60611, USA

Abstract

The espins are a family of multifunctional actin cytoskeletal proteins. They are present in hair cell stereocilia and are the target of mutations that cause deafness and vestibular dysfunction. Here, we demonstrate that the different espin isoforms are expressed in complex spatiotemporal patterns during inner ear development. Espin 3 isoforms were prevalent in the epithelium of the otic pit, otocyst and membranous labyrinth as they underwent morphogenesis. This espin was down-regulated ahead of hair cell differentiation and during neuroblast delamination. Espin also accumulated in the epithelium of branchial clefts and pharyngeal pouches and during branching morphogenesis in other embryonic epithelial tissues, suggesting general roles for espins in epithelial morphogenesis. Espin reappeared later in inner ear development in differentiating hair cells. Its levels and compartmentalization to stereocilia increased during the formation and maturation of stereociliary bundles. Late in embryonic development espin was also present in a tail-like process that emanated from the hair cell base. Increases in the levels of espin 1 and espin 4 isoforms correlated with stereocilium elongation and maturation in the vestibular system and cochlea, respectively. Our results suggest that the different espin isoforms play specific roles in actin cytoskeletal regulation during epithelial morphogenesis and hair cell differentiation.

Keywords

otocyst; hair cell; stereocilia; actin; branching morphogenesis; vestibulocochlear ganglion; neuroblast; cytocaud; lung; lacrimal gland

Introduction

The development of the inner ear involves a precisely coordinated program of tissue morphogenesis and cytodifferentiation (Barald and Kelley, 2004; Fekete and Wu, 2002; Fritzsch and Beisel, 2003; Frolenkov et al., 2004). The otic placode becomes the otocyst, which – through the sprouting, elongation and remodeling of multiple epithelial outgrowths

Correspondence: Dr. James R. Bartles, Dept. of Cell and Molecular Biology, Ward Building 11-185, Northwestern University Feinberg School of Medicine, 303 East Chicago Avenue, Chicago, IL 60611, USA, Phone: 312-503-1545; FAX: 312-503-7912, E-mail: j-bartles@northwestern.edu.

– gives rise to the labyrinth that houses the organs of auditory and vestibular sense. These organs, which consist of innervated sensory hair cells (HCs) interspersed among supporting cells in precise arrangements, arise through a stereotyped pattern of cellular differentiation involving inductive and inhibitory signals (Barald and Kelley, 2004; Woods et al., 2004). Atop each sensory HC is an oriented staircase-like collection of cross-linked stereocilia – the stereociliary bundle – which makes the HC mechanosensitive to sound, motion or gravity (Frolenkov et al., 2004). Stereocilia are formed in part through a programmed elongation and thickening of microvillus-like precursors that mirrors changes in the dimensions of the parallel-actin-bundle scaffold at their core (Tilney et al., 1992; Frolenkov et al., 2004).

One group of proteins implicated in stereocilium integrity and size regulation is the espins. Identified originally as potent actin-bundling proteins (Bartles et al., 1996; 1998), espins are localized to the parallel actin bundle at the core of HC stereocilia and the microvilli of other sensory cells (Sekerková et al., 2004) and are the target of deafness mutations in mice (the jerker mutation) (Zheng et al., 2000) and humans (Naz et al., 2004; Donaudy et al., 2005). In addition to bundling actin filaments in a Ca^{2+}-resistant fashion (Bartles et al., 1998; Chen et al., 1999; Sekerková et al., 2004), espins cause a dramatic, concentration-dependent increase in the steady-state length of microvilli in transfected epithelial cells (Loomis et al., 2003; Sekerková et al., 2004). Likewise, in cultured organ of Corti, espin over-expression increases the length of stereocilia and microvilli in transfected HCs and supporting cells, respectively (Rzadzinska et al., 2005). Since endogenous espin protein levels are higher in HCs with longer stereocilia (Loomis et al., 2003), and homozygous jerker mice, which are deficient in espin protein in all tissues examined (Zheng et al., 2000), have abnormally short hair cell stereocilia (Sjöström and Anniko, 1992a; 1992b; Rzadzinska et al., 2005), we have hypothesized that espins function in part to increase and maintain the steadystate length of stereocilia (Loomis et al., 2003).

Espins are encoded by a single gene, but are produced in multiple isoforms that differ markedly in their size and in their constellation of biological activities and ligand-binding sites (Sekerková et al., 2004) as illustrated in Figs. 1A,B. Different transcriptional start sites distinguish four major espin isoform size classes, which range from ~110 kDa to ~25 kDa in apparent molecular mass and are designated 1–4, in order of decreasing size; splice variants are further specified alphabetically (Sekerková et al., 2004). All espin isoforms contain a 116-amino acid C-terminal actin-bundling module, which is necessary and sufficient for actin-bundling and microvillar elongation activities (Bartles et al., 1998; Loomis et al., 2003), and a Wiskott-Aldrich Syndrome protein homology 2 (WH2) domain that can bind actin monomer (Sekerková et al., 2004). However, the isoforms contain different N-terminal peptides that can include multiple ankyrin-like repeats, an additional binding site for F-actin, a binding site for phosphatidylinositol 4,5-bisphosphate (PIP2) and one or more proline-rich peptides, which can bind profilins or certain Src homology 3 (SH3) domains (Chen et al., 1999; Sekerková et al., 2004). Thus, espins are more than actin-bundling proteins; they are multifunctional actin cytoskeletal regulatory proteins. Moreover, because of their differences in structure, the espin isoforms have the potential to differentially influence the organization, dimensions, dynamics and signaling properties of actin cytoskeletal structures. Consistent with this notion, different cell types express specific espin isoforms or combinations of isoforms (Bartles et al., 1998; Sekerková et al., 2003; 2004). For example, in adult rats cochlear HCs contain espin 3 and espin 4 isoforms, whereas espin 1 is restricted to vestibular HCs (Sekerková et al., 2004).

Li et al. (2004) examined overall espin localization during HC development in chick embryos and found espin to be colocalized with F-actin in HC stereocilia during the initiation and growth of stereociliary bundles. Stereociliogenesis in rodents differs from that in chicks in that it is more difficult to resolve into discrete stages and extends into the first

2–3 weeks of postnatal development (Roth and Bruns, 1992b; Kaltenbach et al., 1994; Frolenkov et al., 2004; Kikkawa et al., 2005; Goodyear et al., 2005; Michel et al., 2005; Lagziel et al., 2005). In this regard, it is noteworthy that the stereociliary shortening and degeneration reported for the cochlear HCs of homozygous jerker mice becomes pronounced around postnatal day 10 (P10) and beyond (Sjöström and Anniko, 1992a; 1992b; Rzadzinska et al., 2005). To better understand the roles of espin and determine how espin gene mutations cause deafness and vestibular dysfunction in mammals, we undertook this study of espin isoform expression during embryonic and postnatal ear development in the rat. We found that marked changes in espin isoform expression not only surrounded stereociliogenesis in HCs, but were also associated with the epithelial morphogenesis that occurs during the early development of the inner ear and other organs and with the maturation of HC stereocilia during early postnatal life.

Materials and methods

Animals

Sprague-Dawley rats and jerker mice were either purchased from a commercial supplier or bred in the Center for Comparative Medicine at Northwestern University. All experiments conformed to protocols approved by the Northwestern University Animal Care and Use Committee and followed guidelines issued by the National Institutes of Health. The day of the vaginal plug was counted as embryonic day 0 (E0). To ensure accurate timing, we counted somite number in early embryos and measured the crown-rump length of unfixed embryos. These data were matched with rat developmental stages (http://anatomy.med.unsw.edu.au/cbl/embryo/OtherEmb/Rat.htm) in half-day increments (e.g. E10, E10.5, E11, etc.) and compared to mouse developmental stages (Kaufman, 1992), assuming a 1.5–2 d difference. Mouse embryos obtained from the mating of homozygous jerker males with heterozygous jerker females were genotyped by DNA sequence analysis of PCR products obtained from genomic DNA isolated from amniotic sac (Zheng et al., 2000).

Timed-pregnant dams were deeply anesthetized with sodium pentobarbital (60 mg/kg). The embryos were harvested by cesarean section and fixed in 2% paraformaldehyde (PFA) for 0.5–1 h, depending on the embryonic age, with the younger embryos being fixed for a shorter time. To facilitate labeling with mouse antibody to class III β-tubulin, the fixation time was cut approximately in half to achieve a lower degree of fixation. The inner ear and cochlear surface preparations were removed by dissection from embryos older than E14 and E16, respectively. Postnatal rats (P0–P16) were perfused transcardially with 4% PFA. Bony labyrinths were removed, decalcified in 8% EDTA (1–12 d, depending upon age), and cochlear surface preparations were removed by dissection. Developing lungs and lacrimal gland regions were removed by dissection and fixed with 2% PFA.

Immunohistochemistry

Whole embryos, embryonic inner ear preparations, lungs and lacrimal gland regions were pretreated with dimethylsulfoxide (DMSO), 30% H_2O_2 and methanol 1:1:4 (vol/vol) for 1 h and then with 3% normal goat serum (NGS), 1% bovine serum albumin (BSA) in TBS (100 mM Tris-HCl, 150 mM NaCl, pH 7.6), 2% Triton X-100, 0.2% DMSO for 1 h. These embryos were incubated with affinity purified rabbit pan-espin antibody or preimmune IgG diluted in TBS, 2% Triton X-100, 0.2% DMSO containing 1% NGS, 1% BSA, and 0.08% NaN_3 overnight at room temperature with gentle shaking. The espin antibody, which was raised against purified recombinant rat espin 2B and affinity purified on columns of rat espin 2B-Sepharose 4B, is known to react with all espin isoforms (Sekerková et al., 2003; 2004). After 6–7 1-h rinses with TBS, 0.2% Triton X-100 at room temperature, the embryos were

incubated with biotinylated donkey antirabbit IgG (Amersham Biosciences, Piscataway, NJ) in TBS, 2% Triton X-100, 0.2% DMSO containing 1% NGS and 1% BSA overnight at 4°C. After rinsing as before, the samples were incubated with avidin-biotin complex (ABC Elite kit; Vector, Burlingame, CA) overnight at 4°C, and the bound antibody was visualized with diaminobenzidine.

Slide-mounted cryostat sections (25 μm) and free-floating cochlear surface preparations were labeled with the espin antibody, with or without mouse antibody to class III β-tubulin (TuJ1; gift of Dr. A. Frankfurter, University of Virginia, Charlottesville, VA) or calretinin (Chemicon, Temecula, CA), using standard immunostaining protocols for light and fluorescence microscopy (Sekerková et al., 2003; 2004). Bound antibodies were visualized by the ABC method (Vector Elite kit) or by secondary antibodies labeled with Alexa 488 or 594 (Molecular Probes, Eugene, OR). F-actin was visualized using Alexa 488-phalloidin (Molecular Probes).

Confocal analysis of espin levels in cochlear HCs

To compare relative espin levels in HCs at different positions from base to apex along the cochlear spiral, cochlear surface preparations from P1 and P12 animals were stained with espin antibody and Alexa 488-labeled secondary antibody (Molecular Probes). Confocal images representing z-stacks of the entire stereociliary region were taken from two different positions along the cochlear spiral: one ~30% from the base and another ~70% from the base. The range of signal intensities was so large, especially in the P12 specimens, that to detect the lowest signal intensities in the outer hair cells (OHCs) at the ~30% position the gain had to be set in such a way that the highest signal intensities were oversaturated in the figures (e.g., see Fig. 7G). Because of this and other technical limitations, this method can reveal major qualitative differences in espin levels in HCs at different locations, but cannot rigorously quantify these levels or the concentration of espin per unit length along individual stereocilia. Color-scale coding of espin immunofluorescence intensities was carried out using the Zeiss LSM 510 software package (Loomis et al., 2003).

Western blot analysis

To examine developmental trends in whole embryos from E10.5 through E12.5 (Fig. 1M), samples were prepared using approximately equal wet masses of whole embryos. This involved the use of 2–5 embryos for each specimen, depending on age. To examine developmental trends in inner ear from E10.5 through P15 (Figs. 7A,B), samples were prepared using approximately equal masses of tissue from the following: E10.5, 6 anterior embryo halves; E14, 4 otic regions (inner ear together with some surrounding tissue); E18 and beyond, 4 bony labyrinths. To examine developmental trends in inner ear from P2 through P10 (Fig. 7C), samples were prepared using approximately equal masses of tissue consisting of 4 bony labyrinths.

Embryos, embryo regions or crushed bony labyrinths were homogenized in 20 volumes (ml/g of wet tissue) of 0.25 M sucrose, 3 mM imidazole-HCl, pH 7.4, containing 1 mM phenylmethylsulfonyl fluoride at 4°C using a 5-ml Potter-Elvehjem homogenizer (8 strokes, 3000 rpm) and immediately extracted at a concentration of ~40 mg wet tissue/ml by heating at 100°C in SDS gel sample buffer for 3 min, with intermittent agitation on a vortex mixer. The samples were centrifuged at 16,000 × g in a microcentrifuge, and the resulting supernates were resolved in SDS gels and analyzed on western blots using the ECL system (Amersham Biosciences), with or without prior stripping according to the procedure recommended by the manufacturer.

Results

Espin expression during the early stages of inner ear development and neuroblast delamination

Whole rat embryos labeled with the affinity purified pan-espin antibody showed an unexpectedly intense immunostaining of the otic pit and otocyst. This was observed from the first time point examined, E10 (Fig. 1C), and persisted through the early morphogenesis of the otocyst, encompassing the outgrowth of the endolymphatic duct, vestibular canal pouches, and cochlear duct (Figs. 1C–I). We also noticed significant staining of the branchial clefts (Figs. 1C–F). This latter staining decreased in intensity coincident with the appearance of provisional structures, such as the auditory hillocks (Fig. 1I).

The immunostaining observed in the embryos was shown to be specific in two types of control experiments. It was not observed when the espin antibody was replaced by preimmune IgG (Fig. 1J) or omitted (not shown). Thus, the espin antibody was required to observe this immunostaining. We also compared the level of immunostaining in mouse embryos from the same litter that were determined to be heterozygous and homozygous for the jerker mutation by genotyping. We have already shown that, as a result of the jerker mutation in the mouse espin gene, homozygous jerker mice lack espin protein in all tissues that would normally express espins – such as testis, kidney, and inner ear – whereas the tissues of jerker heterozygotes contain roughly half the normal amount of espin protein (Zheng et al., 2000). At E10 in the mouse, which is comparable to E11.5 in rat, immunostaining was detected in the otocyst and branchial clefts of the heterozygous jerker mouse embryos (Fig. 1K), but was not detected in these structures in homozygous jerker mouse embryo littermates (Fig. 1L). This further confirmed that the immunostaining we observed in the embryos was attributed to espin protein.

Comparison of duplicate western blots of whole rat embryos labeled with the espin antibody or preimmune IgG indicated the presence of specifically labeled bands corresponding to major espin isoform classes (Fig. 1M), which because of their differences in size (Fig. 1A) can readily be distinguished on the basis of apparent molecular mass (Sekerková et al., 2004). The espin 3 isoforms, which migrate as multiple bands at ~32–35 kDa, predominated at these stages (Fig. 1M). Comparisons of equal masses of embryos from different stages showed an ~5-fold increase in the level of the espin 3 isoforms between E10.5 and E12.5 (Fig. 1M). Smaller amounts of specific labeling were observed for espin 2 (~60 kDa), and faint bands corresponding to espin 1 (~110 kDa) could be detected. Espin 4, which migrates as multiple bands at ~22–28 kDa is not shown in Fig. 1M, because it was obscured by nonspecifically labeled bands in the whole-embryo specimens. However, faint bands corresponding to espin 4 could be discerned in samples prepared from the anterior half of embryos at E10.5 (see Fig. 7B, below).

The analysis of rat embryo sections confirmed the presence of high levels of specific staining with the espin antibody in the epithelium of the otocyst and developing membranous labyrinth (Fig. 2). From E10 through E13, the espin antibody strongly labeled the entire otic epithelium (Figs. 2A–H). When examined by confocal microscopy, every cell in the otic epithelium showed cytoplasmic staining (FIG. 2C). In addition, staining was enriched in the microvillar zone at the otocyst lumen (Fig. 2C, arrowheads). In sections, the immunostaining observed in the branchial clefts of embryo whole-mounts (Figs. 1C–F) was localized to the epithelial cells that line the clefts (Fig. 2A). In addition, the sections revealed an even stronger immunostaining of the epithelium lining the pharyngeal pouches (Figs. 2A,B).

We observed a decrease in espin immunostaining during the delamination of neuroblasts from the otocyst (Figs. 2A,B) and cochlear duct (Figs. 2D,E) to assemble the vestibulocochlear (VIIIth-cranial) ganglion (VCG). In its early stages (e.g., at E11–E12), the VCG is combined with the facial-sensory (VIIth-cranial) ganglion to form the acousticofacial preganglion complex (AFG) (Kaufman and Bard, 1999; Rubel and Fritzsch, 2002). Careful inspection of the border between the AFG and otocyst (Figs. 2A,B), and later between the VCG and cochlear duct (Figs. 2D,E), revealed groups of cells of intermediate immunostaining intensity, suggesting that espin protein levels underwent a progressive decrease upon delamination. The border between the first pharyngeal pouch and the AFG exhibited a similar appearance (Figs. 2A,B).

Neuroblasts were identified by labeling with the TuJ1 monoclonal antibody against neuron-specific class III β-tubulin, which is sensitive to the degree of fixation (Molea et al., 1999; Stone et al., 2003). With our standard fixation conditions, TuJ1 staining was largely confined to the AFG and difficult to detect within the otic epithelium (Fig. 2G). However, when specimens were fixed for approximately one-half as long, it was possible to detect TuJ1-positive neuroblasts in the epithelium of the medial and ventral walls of the otocyst (Figs. 2H–L, refer to diagram in Fig. 2F). Double labeling with the espin and TuJ1 antibodies revealed that the general cytoplasmic staining with espin antibody within the otic epithelium extended to the TuJ1-positive neuroblasts (Figs. 2J–L). The graded reduction in espin immunostaining intensity observed during neuroblast delamination (Figs. 2A,B) was substantiated by immunofluorescence in sections cut at different levels (refer to Fig. 2F) to reveal the otocyst (Fig. 2K), the border region (Fig. 2M, asterisks) and the AFG (Fig. 2O, asterisks).

Espin expression during the intermediate stages of inner ear development and during epithelial morphogenesis in other organs

The epithelium of the otocyst and developing labyrinth continued to show relatively homogeneous cytoplasmic staining with the espin antibody into the intermediate stages of inner ear development. Although increasingly difficult to visualize in whole embryos beyond E13.5 (not shown), this immunostaining was clearly detected in the various parts of the developing labyrinth in whole-mounts of rat embryonic inner ear (Fig. 3). In specimens from E14.5 through E16.5, the espin antibody labeled the semicircular canals, including their ampullar primordia, the utriculo-saccular region, the cochlea and the endolymphatic duct and sac (Figs. 3A–F). During the interval of E14.5 through E16.5, there was a reduction in the overall level of staining in the developing labyrinth and an enrichment in the vestibular sensory endorgans and the modiolar face of the developing cochlea (Figs. 3A–I, and see below). At E17 and beyond, it became necessary to expose the membranous labyrinth by removing the capsule to gain sufficient access (Figs. 3G–I). By this stage, patches of HCs with espin antibody-positive stereociliary bundles were already evident in the sensory endorgans of the vestibular system (Figs. 3G,H), while the surrounding epithelium was relatively free of staining (Figs. 3G–I). The labeled stereociliary bundles are easier to discern in sections (e.g., see Figs. 4E–G, below). By E16.5, the staining of the endolymphatic duct and sac had decreased and become patchy (Figs. 3F,I).

These trends in immunostaining were confirmed in sections of the developing membranous labyrinth (Fig. 4) and in cochlear surface preparations (Fig. 5), both of which afforded greater resolution. The general staining of the epithelium in the developing vestibular system had decreased substantially by the time the first HCs could be detected in its sensory endorgans, e.g., at E14 in the macula (Figs. 4A–D). The general epithelial cell staining in the developing cochlea persisted longer and at E16 began to disappear from the prospective sensory zone in the dorsal wall of the cochlear duct (Figs. 4I,J). This zone grew in size, so that by E17 it included the lesser epithelial ridge and much of the adjoining greater epithelial

ridge (Fig. 4K). The decrease in espin antibody staining encompassed the whole length of the cochlear duct (Fig 4I) and preceded the appearance of espin-positive cochlear HCs (Fig. 4I–K, Fig. 5A–H). Although at E16 some espin immunostaining was retained at the luminal surface of cochlear epithelial cells (Fig. 4I,J, Fig. 5D,M), this, too, had decreased by E17/E18 (Fig. 4K, Fig. 5F). These changes caused the general immunostaining in the cochlea to appear increasingly enriched in the epithelial cells on the modiolar side of the greater epithelial ridge (Fig. 4K, Fig. 5F,H,J,L). These cells will continue to undergo morphogenesis to sculpt the inner sulcus and contribute to spiral limbus epithelium (Roth and Bruns, 1992a;Souter et al., 1997;Rau et al., 1999). Like the espin-positive epithelial cells observed throughout the labyrinth earlier in development (Fig. 2C), the immunostaining in these cells appeared to be distributed throughout the cytoplasm (Figs. 5N,O). Consistent with the base-to-apex gradient of maturation in the cochlea (Kaltenbach and Falzarano, 1994;Kaltenbach et al., 1994;Zine and Romand, 1996), the cytoplasmic immunostaining of these epithelial cells gradually declined in a base-to-apex gradient from E16 through the first postnatal week. At P0/P1 low levels of immunostaining could still be detected (Figs. 5J,L,O,P, asterisks), especially in apical regions (asterisk in Fig. 5P) that contained immature HCs (Fig. 5R). By P8 any general epithelial cell staining was difficult to distinguish from background (not shown).

The epithelial cells of the otic pit, otocyst and developing labyrinth displayed strong general staining with espin antibody during periods of extensive epithelial morphogenesis. High levels of specific staining with the espin antibody were found in other instances of epithelial morphogenesis in these embryos. Two examples are shown in Figure 6: developing lacrimal gland (Figs. 6A–D) and lung (Figs. 6F–I). In both embryonic structures, high levels of immunostaining were observed throughout the epithelial tree during periods of growth via branching epithelial morphogenesis (Figs. 6A–D,G–I). As was the case in the developing inner ear, this general immunostaining was distributed throughout the epithelium (illustrated clearly for lung in Fig. 6F), and the level of staining decreased substantially as these structures reached maturity (Figs. 6E,J). These results suggested that increased expression of espin protein was a common feature of epithelial morphogenesis during embryonic development.

Espin expression during hair cell differentiation: stereociliogenesis and an espin-rich basal process

When first detected during inner ear development, HCs showed enhanced staining with the espin antibody relative to neighboring epithelial cells and a pattern of staining that differed from those of their progenitors and mature HCs. This is illustrated for early HCs in the macula at E14 in Figs. 4A–D. These cells, which are double-labeled with antibody to calretinin, an early marker for vestibular HCs (Zheng and Gao, 1997), showed enrichment of espin antibody staining in an apical tuft of presumptive microvilli/immature stereocilia and throughout the cytoplasm in the apical part of the cell. HCs arose in the vestibular maculae ~2 d before they appeared in the cochlea. At E16, a single row of inner HCs (IHCs) was first detected in the mid-basal part of the cochlea (Fig. 4I,J, Fig. 5A–C). These cells, which appeared in the zone showing a marked reduction in general cytoplasmic staining (Figs. 4I,J), exhibited a pattern of staining similar to that for early vestibular HCs (Fig. 4B), with enrichment in an apical tuft of microvilli/immature stereocilia and in the apical cytoplasm (Fig. 4J). However, the cytoplasmic staining in early cochlear HCs appeared lower than that in early vestibular HCs (Fig. 4A,B,J). When viewed from above in cochlear surface preparations, increased immunostaining in a crown of apical microvilli/immature stereocilia could also be discerned (Figs. 5A–C). By E18, one row of IHCs and multiple rows of OHCs were detected in the mid-basal region (Fig. 4L, Fig. 5E–G). As noted previously (Romand et al., 1993), staining for F-actin with fluorescent phalloidin (green in Fig. 4L) was

exceptionally intense all along the luminal face of the epithelium in the developing organ of Corti and neighboring greater epithelial ridge at E18. Whether in the vestibular system (Figs. 4E–H) or in the cochlea (Fig. 4L,M,Fig. 5G,K,S), as HCs continued to differentiate, the immunostaining of stereocilia became more pronounced, and the level of cytoplasmic staining decreased dramatically. HC appearance and the progressive enrichment of immunostaining in stereocilia proceeded in a base-apex gradient along the cochlear spiral (Figs. 5A–S). Therefore, partially differentiated HCs could still detected at the extreme apex at P1 (Figs. 5P,R). Segments showing an additional row of OHCs could also be found at P1 (Figs. 5P,S), and these supernumerary OHCs also showed enriched immunostaining in their stereocilia (Fig. 5S).

In our analysis of espin antibody staining during HC differentiation, we noted a peculiar, espin antibody-positive, tail-like structure that emanated from the basal surface of vestibular and cochlear HCs and extended toward the basement membrane. This espin-rich basal process was detected at E18 in the vestibular system (Figs. 4H,N, arrows) and cochlea (Figs. 4L,M, arrows). Examples can also be seen upon close-up inspection of Fig. 4G (arrows) and Figs. 5G,H (yellow arrows). This process, which was distinct from nerve fibers, as revealed by labeling with TuJ1 tubulin antibody (Fig. 4N), was transient in that it was not detected before E17 or at P0 and beyond.

Differential expression of espin isoforms during embryonic development and postnatal maturation

Western blot analysis revealed changes in espin isoform expression in the rat inner ear during embryonic development and postnatal maturation (Figs. 7A–C). The pattern of expression seen previously in the adult inner ear, characterized by large amounts of the espin 1 isoform and lower levels of the espin 3 and 4 isoforms (Sekerková et al., 2004), was established by P15 (Fig. 7B). The espin 2 and 3 isoforms, which were also detected on western blots of whole embryos (Fig. 1M), predominated in embryonic inner ear until E20. Between E14 through P15, the level of the espin 2 decreased, and the level of the espin 3 increased (Figs. 7B). The accumulation of the espin 1 isoform, which is confined to vestibular HCs in adults (Sekerková et al., 2004), occurred during late embryonic and early postnatal development (Figs. 7B,C). Consistent with the early maturation of vestibular HCs (Mbiene, et al., 1984; Lim and Anniko, 1985; Zheng and Gao, 1997), the concentration of espin 1 increased dramatically between E20 and P0 and continued to increase during the first several postnatal days, reaching a maximum around P6 (Figs. 7B,C). In contrast, the concentration of espin 4 was low through P0, remained relatively low until the middle of the first postnatal week and then increased from P6 through P10 (Figs. 7B,C). This latter time period is associated with the postnatal maturation of stereociliary bundles in the cochlea (Roth and Bruns, 1992b; Kaltenbach et al., 1994; Zine and Romand, 1996; Frolenkov et al., 2004; Kikkawa et al., 2005; Goodyear et al., 2005; Michel et al., 2005; Lagziel et al., 2005).

One aspect of postnatal maturation in the cochlea is the differential elongation of stereocilia to achieve the increasing gradient in stereocilium length observed from base to the apex along the cochlear spiral in adults (Roth and Bruns, 1992b; Kaltenbach et al., 1994). We showed previously that increasing the level of espin in transfected epithelial cells causes a concentration-dependent elongation of their microvilli and that in adult rats there is an increasing gradient in HC espin level from base to apex along the cochlear spiral that could account for this increasing gradient of stereocilium length (Loomis et al., 2003). To determine if this gradient in HC espin level arose during postnatal maturation, we employed the same confocal immunofluorescence approach to compare espin levels in HCs positioned ~30% and ~70% from the cochlear base at P1 and P12. This assay takes advantage of the fact that espins are so highly concentrated in stereocilia that the overall immunofluorescence signal intensity in the stereociliary bundle can be taken as a relative measure of total HC

espin level (Loomis et al., 2003). At P1, a time prior to postnatal stereocilium elongation (Roth and Bruns, 1992b; Kaltenbach et al., 1994), HCs positioned at the ~30% and ~70% positions showed relatively similar levels of espin immunofluorescence (Figs. 7D,E,D',E'). In contrast, at P12, when the increasing gradient of stereociliary lengths along the cochlear spiral is already largely established (Roth and Bruns, 1992b; Kaltenbach et al., 1994), HCs positioned at the ~70% position showed a more intense espin immunofluorescence signal than those at the ~30% position (Figs. 7F,G,F',G'). This difference was especially noticeable for OHCs (Figs. 7F,G,F',G', arrowheads) and is in general agreement with our earlier studies in adult rats (Loomis et al., 2003). IHCs also showed a more intense signal at the ~70% position than at the ~30% position at P12, but this difference cannot be discerned in the figure, because at this exposure the signals from the IHCs are over-saturated (Figs. 7F,G,F',G', arrows). Moreover, as in adults (Loomis et al., 2003), we observed a greater signal intensity for IHCs than OHCs (especially noticeable in Figs. 7F,F'), which correlates with known differences in stereocilium length (Roth and Bruns, 1992b; Kaltenbach et al., 1994). These results suggested that postnatal increases in espin levels in cochlear HCs, which coincide with the increase in the concentration of espin 4 isoforms on western blots (Figs. 7B,C), could account for the differential elongation of HC stereocilia along the cochlear spiral that takes place during early postnatal life.

Discussion

We have determined that the structurally and functionally distinct isoforms of the espin family of actin cytoskeletal proteins are expressed in complex spatiotemporal patterns throughout rodent inner ear development, from the time of otic pit formation through the postnatal maturation of cochlear HC stereocilia. Our findings implicate specific espin isoforms in stereocilium elongation and maturation in the cochlea and vestibular system, draw attention to a previously unrecognized structural specialization of differentiating HCs – the espin-rich basal process – and suggest novel roles for espins as actin cytoskeletal regulators during epithelial morphogenesis in the developing inner ear and in other organs.

The early espin protein expression we detected throughout the epithelium of the rodent otic pit, otocyst and developing membranous labyrinth was totally unexpected, because previous work on inner ear espins examined either mature HCs in rodents or chickens (Zheng et al., 2000; Loomis et al., 2003) or HC stereociliogenesis in chick embryos (Li et al., 2004). Using complementary approaches, we demonstrated that the immunostaining of these embryonic otic progenitors, which included early neuroblasts, reflected the presence of espin proteins – especially the espin 3 isoforms, which differ significantly from the other isoforms in structure and certain aspects of their biological activity (Figs. 1A,B). For example, the espin 3 isoforms inhibit actin polymerization in vitro, contain only one profilin-binding proline-rich peptide and do not bind to phospholipid membrane vesicles containing PIP2. The fact that espins are also expressed early in inner ear development could have some implications for their use as cell lineage or differentiation markers. Interestingly, this early espin protein expression did not conform to the compartment boundaries that exist within the otic epithelium, as revealed by the localization of transcription factor mRNAs (Fekete and Wu, 2002; Lin et al., 2005). Instead, it was distributed uniformly throughout the epithelium, suggesting a global role for these espin proteins in inner ear morphogenesis.

Our analysis of espins in embryonic development led to the discovery that espin protein expression was associated with multiple instances of epithelial morphogenesis. In the context of inner ear development, espin proteins were detected in embryonic otic epithelium during the invagination of the otic pit, the sprouting and elongation of the endolymphatic and cochlear ducts, and the formation and remodeling of the vestibular canal pouches. But, in addition, espin protein accumulation was noted in a variety of other embryonic epithelia

as they underwent morphogenesis. Here, we presented data on four such structures: the lacrimal gland and lung, both of which undergo branching morphogenesis (Dean et al., 2004; Chuang and McMahon, 2003), and the branchial clefts and pharyngeal pouches, which exhibit extensive remodeling during embryogenesis (Graham, 2003; Quinlan et al., 2004). This raises the possibility that espin protein expression is increased by common signals and mechanisms that mediate epithelial morphogenesis in these diverse locations (Davies, 2002). Epithelial morphogenesis typically involves changes in cell shape, adhesion and polarity, often in conjunction with cell migration or proliferation – any of which can depend upon the actin cytoskeleton (Schöck and Perrimon, 2002; Pilot and Lecuit, 2005). Thus, in view of the multiple ways that espins can interact with actin and influence the actin cytoskeleton (Sekerková et al., 2004), we propose that the espins contribute to actin cytoskeletal regulation during epithelial morphogenesis. Consistent with a role in epithelial morphogenesis, the levels of espin decreased dramatically upon completion of morphogenesis in these various epithelial tissues or, in the case of delaminating neuroblasts, upon exit from the epithelium and further differentiation.

Unlike the espins of most adult tissues, a large fraction of the espin present during epithelial morphogenesis in embryos was not obviously associated with cellular structures known to contain relatively large parallel actin bundles, such as stereocilia, microvilli or Sertoli cell junctional plaques (Zheng et al., 2000; Bartles et al., 1998; Chen et al., 1999). Instead, this espin appeared to be distributed relatively diffusely throughout the cytoplasm of the epithelial cell. This more diffusely localized pool of espin proteins might be carrying out one or more of the other actin cytoskeletal regulatory functions for which espins are equipped (Sekerková et al., 2004). In the context of epithelial morphogenesis, this could involve roles in apical constriction, junction remodeling, cell columnarization, cell flattening, or basal protrusion (Schöck and Perrimon, 2002; Pilot and Lecuit, 2005). A web of cytoplasmic actin cables interconnecting N-cadherin-containing adherens junctions has recently been implicated in pharyngeal pouch morphogenesis (Quinlan et al., 2004). Beyond the shortening and degeneration of HC stereocilia noted in early postnatal life (Sjöström and Anniko, 1992a; 1992b) and some problems with the tectorial membrane (Deol, 1954), morphogenetic defects have not yet been reported for the epithelial tissues of homozygous jerker mice, which we have shown to be deficient in espin proteins in every tissue examined that would normally express an espin protein (Zheng et al., 2000; and Fig. 1L). Although we noted no major anatomical defects in jerker mouse embryo whole-mounts at E10 (Fig. 1K,L), the widespread distribution of espin proteins throughout in the developing inner ear and in other embryonic epithelial tissues warrants a detailed search for additional defects in the jerker mouse.

Espin protein expression was also observed later in inner ear development during HC differentiation. Because this espin was detected in HCs following down-regulation of the cytoplasmic espin immunostaining in the prospective sensory regions of the labyrinth, it likely represents a second wave of espin protein accumulation. Unlike the initial wave of espin protein accumulation, this second wave takes place in a highly specific subset of cells within the labyrinth. In agreement with the work of Li et al. (2004) in chick embryos, this espin also proved to be an early marker of differentiating HCs in the cochlea and vestibular system of mammals, and its levels and extent of compartmentalization to stereocilia increased throughout stereociliogenesis. This would be consistent with the roles proposed for espins in stereocilium formation and elongation (Loomis et al., 2003; Li et al., 2004; Rzadzinska et al., 2005). Beyond documenting the parallels in stereociliogenesis between rodents and chickens, our experiments identified two novel aspects of espin expression during HC differentiation: the presence of an espin-rich, tail-like process and the differential expression of espin isoforms that accompanies late embryonic and early postnatal development.

In addition to being localized to the stereocilia of differentiating HCs, we noticed an espin-containing, tail-like process that emanated from the basal surface HCs around E18. To our knowledge, this is the first report of this structure, which may have been overlooked because of its narrow diameter or the absence of a suitable protein marker. The espin-rich basal process was reminiscent of the cytocaud, an actin-rich protrusion that extends basally from the IHCs and type-I vestibular HCs of adult pirouette and shaker-2 mice (Beyer et al., 2000) and the type-I vestibular HCs of the waltzing guinea pig (Kanzaki et al., 2002). Thus, our findings raise the possibility that the cytocaud pathology observed in association with these different deafness mutations results from the aberrant retention or stabilization of a cellular process that is transiently present during the differentiation of normal HCs. The source and structural organization of the espin-rich basal process are currently under investigation.

Consistent with its proposed role in stereocilium elongation (Loomis et al., 2003), the espin expressed during the second wave of expression continued to accumulate in HC stereocilia, and its levels continued to increase into the first 1–2 weeks of postnatal life coincident with stereocilium elongation and maturation in rodents (Roth and Bruns, 1992b; Kaltenbach et al., 1994; Zine and Romand, 1996; Frolenkov et al., 2004; Kikkawa et al., 2005; Goodyear et al., 2005; Michel et al., 2005; Lagziel et al., 2005). This increase in espin protein level involved a surprisingly complex pattern of expression of the different isoforms. The espin 3 isoforms were retained throughout inner ear development, whereas the levels of espin 2 declined before birth. The levels of the two other espin isoform size classes found in the inner ears of adults – espin 1 and espin 4 – exhibited increases at widely different times during stereocilium maturation. The late embryonic and early postnatal increase in the level of espin 1 likely surrounds the maturation of vestibular HC stereocilia, both on the basis of timing (Mbiene, et al., 1984; Lim and Anniko, 1985; Zheng and Gao, 1997) and because espin 1 is confined to the stereocilia of vestibular HCs in adults (Sekerková et al., 2004). A major difference between espin 1 and the other espin isoforms is its N-terminal eight ankyrin-like repeats (Fig. 1A), which could mediate protein-protein interactions (Chen et al., 1999). The relatively late timing of the increase in the espin 4 isoforms (P6–P10) suggests that these smallest espin isoforms mediate the postnatal elongation of stereocilia that establishes the increasing gradient in stereocilium length from base to apex along the cochlear spiral (Roth and Bruns, 1992b; Kaltenbach et al., 1994). The espin 4 isoforms could also be involved in other aspects of cochlear stereociliary bundle maturation known to take place during this interval, such as staircase assembly or the formation and remodeling of stereociliary links (Roth and Bruns, 1992b; Kaltenbach et al., 1994; Zine and Romand, 1996; Frolenkov et al., 2004; Kikkawa et al., 2005; Goodyear et al., 2005; Michel et al., 2005; Lagziel et al., 2005). In this regard, the shortening and degeneration of stereocilia noted in the cochlear HCs of homozygous jerker mice becomes pronounced around P10 (Sjöström and Anniko, 1992a; 1992b), raising the intriguing possibility that these defects stem primarily from a deficiency of espin 4 isoforms in cochlear HCs.

Acknowledgments

We thank Dr. A. Frankfurter for TuJ1 antibody and an anonymous reviewer for many helpful comments. This work was supported by NIH grant DC004314 to JRB. JRB is a Fellow of the Hugh Knowles Center for Clinical and Basic Science in Hearing and Its Disorders.

References

Barald K, Kelley MW. From placode to polarization: new tunes in inner ear development. Development 2004;131:4119–4130. [PubMed: 15319325]

Bartles JR, Wierda A, Zheng L. Identification and characterization of espin, an actin-binding protein localized to the F-actin-rich junctional plaques of Sertoli cell ectoplasmic specializations. J. Cell Sci 1996;109:1229–1239. [PubMed: 8799813]

Bartles JR, Zheng L, Li A, Wierda A, Chen B. Small espin: a third actin-bundling protein and potential forked protein ortholog in brush border microvilli. J. Cell Biol 1998;143:107–119. [PubMed: 9763424]

Beyer LA, Odeh H, Probst FJ, Lambert EH, Dolan DF, Camper SA, Kohrman D, Rafael Y. Hair cells in the Pirouette and Shaker-2 mutants. J. Neurocytol 2000;29:227–229. [PubMed: 11276175]

Chen B, Li A, Wang D, Wang M, Zheng L, Bartles JR. Espin contains an additional actin-binding site in its N terminus and is a major actin-bundling protein of the Sertoli cell-spermatid ectoplasmic specialization junctional plaque. Mol. Biol. Cell 1999;10:4327–4339. [PubMed: 10588661]

Chuang PT, McMahon AP. Branching morphogenesis of the lung: new molecular insights into an old problem. Trends Cell Biol 2003;13:86–91. [PubMed: 12559759]

Davies JA. Do different branching epithelia use a conserved developmental mechanism? Bioessays 2002;24:937–948. [PubMed: 12325126]

Dean C, Ito M, Makarenkova HP, Faber SC, Lang RA. Bmp7 regulates branching morphogenesis of the lacrimal gland by promoting mesenchymal proliferation and condensation. Development 2004;131:4155–4165. [PubMed: 15280212]

Deol MS. The anomalies of the labyrinth of the mutants varitint-waddler, shaker-2 and jerker in the mouse. J. Genetics 1954;52:562–588.

Donaudy F, Zheng L, Ficarella R, Ballana E, Carella M, Melchonida S, Estivill X, Bartles JR, Gasparini P. Espin gene (*ESPN*) mutations associated with autosomal dominant hearing loss cause defects in microvillar elongation or organization. J. Med. Genet. 2005 in press. Published online 1 June 2005.

Fekete DM, Wu DK. Revisiting cell fate specification in the inner ear. Curr. Opin. Neurobiol 2002;12:35–42. [PubMed: 11861162]

Frolenkov GI, Belyantseva IA, Friedman TB, Griffith AJ. Genetic insights into the morphogenesis of inner ear hair cells. Nat. Rev. Genet 2004;5:489–498. [PubMed: 15211351]

Fritzsch B, Beisel KW. Molecular conservation and novelties in vertebrate ear development. Curr. Top. Dev. Biol 2003;57:1–44. [PubMed: 14674476]

Goodyear RJ, Marcotti W, Kros CJ, Richardson GP. Development and properties of stereociliary link types in hair cells of the mouse cochlea. J. Comp. Neurol 2005;485:75–85. [PubMed: 15776440]

Graham A. Development of the pharyngeal arches. Am. J. Med. Genet. A 2003;119:251–256. [PubMed: 12784288]

Kaltenbach JA, Falzarano PR. Postnatal development of the hamster cochlea. I. Growth of hair cells and the organ of Corti. J. Comp. Neurol 1994;340:87–97. [PubMed: 8176004]

Kaltenbach JA, Falzarano PR, Simpson TH. Postnatal development of the hamster cochlea. II. Growth and differentiation of stereocilia bundles. J. Comp. Neurol 1994;350:187–198. [PubMed: 7884037]

Kanzaki S, Beyer LA, Canlon B, Meixner WM, Raphael Y. The cytocaud: A hair cell pathology in the waltzing guinea pig. Audiol. Neurotol 2002;7:289–297.

Kaufman, MH. The atlas of mouse development. San Diego: Academic Press; 1992.

Kaufman, MH.; Bard, JBL. The anatomical basis of mouse development. San Diego: Academic Press; 1999.

Kikkawa Y, Mburu P, Morse S, Kominami R, Townsend S, Brown SD. Mutant analysis reveals whirlin as a dynamic organizer in the growing hair cell stereocilium. Hum. Mol. Genet 2005;14:391–400. [PubMed: 15590699]

Lagziel A, Ahmed ZM, Schultz JM, Morell RJ, Belyantseva IA, Friedman TB. Spatiotemporal pattern and isoforms of cadherin 23 in wild type and waltzer mice during inner ear hair cell development. Dev. Biol 2005;280:295–306. [PubMed: 15882574]

Li H, Liu H, Balt S, Mann S, Corrales CE, Heller S. Correlation of expression of the actin filament-bundling protein espin with stereociliary bundle formation in the developing inner ear. J. Comp. Neurol 2004;468:125–134. [PubMed: 14648695]

Lim DJ, Anniko M. Developmental morphology of the mouse inner ear. A scanning electron microscopic observation. Acta Otolaryngol. Suppl. (Stockh.) 1985;422:1–69. [PubMed: 3877398]

Lin Z, Cantos R, Patente M, Wu DK. Gbx 2 is required for the morphogenesis of the mouse inner ear: a downstream candidate of hindbrain signaling. Development 2005;132:2309–2318. [PubMed: 15829521]

Loomis PA, Zheng L, Sekerková G, Changyaleket B, Mugnaini E, Bartles JR. Espin cross-links cause the elongation of microvillus-type parallel actin bundles. J. Cell Biol 2003;163:1045–1055. [PubMed: 14657236]

Mbiene J-P, Favre D, Sans A. The pattern of ciliary development in fetal mouse vestibular receptors. A qualitative and quantitative SEM study. Anat. Embryol 1984;170:229–238. [PubMed: 6151813]

Michel V, Goodyear RJ, Weil D, Marcotti W, Perfettini I, Wolfrum U, Kros CJ, Richardson GP, Petit C. Cadherin 23 is a component of the transient lateral links in the developing hair bundles of cochlear sensory hair cells. Dev. Biol 2005;280:281–294. [PubMed: 15882573]

Molea D, Stone JS, Rubel EW. Class III β-tubulin expression in sensory and nonsensory regions of the developing avian inner ear. J. Comp. Neurol 1999;406:183–198. [PubMed: 10096605]

Naz S, Griffith AJ, Riazuddin S, Hampton LL, Battey JF Jr, Khan SN, Riazuddin S, Wilcox ER, Friedman TB. Mutations of ESPN cause autosomal recessive deafness and vestibular dysfunction. J. Med. Genet 2004;41:591–595. [PubMed: 15286153]

Pilot F, Lecuit T. Compartmentalized morphogenesis in epithelia: from cell to tissue shape. Dev. Dyn 2005;232:685–694. [PubMed: 15712202]

Quinlan R, Martin P, Graham A. The role of actin cables in directing the morphogenesis of the pharyngeal pouches. Development 2004;131:593–599. [PubMed: 14711875]

Rau A, Legan PK, Richardson GP. Tectorin mRNA expression is spatially and temporally restricted during mouse inner ear development. J. Comp. Neurol 1999;405:271–280. [PubMed: 10023815]

Romand R, Zine A-E, Hafidi A. Ontogenesis of F-actin in hair cells. Cell Motil. Cytoskel 1993;25:213–222.

Roth B, Bruns V. Postnatal development of the rat organ of Corti. I. General morphology, basilar membrane, tectorial membrane and border cells. Anat. Embryol. (Berl.) 1992a;185:559–569. [PubMed: 1605367]

Roth B, Bruns V. Postnatal development of the rat organ of Corti. II. Hair cell receptors and their supporting elements. Anat. Embryol. (Berl.) 1992b;185:571–581. [PubMed: 1605368]

Rubel EW, Fritzsch B. Auditory system development: primary auditory neurons and their targets. Annu. Rev. Neurosci 2002;25:51–101. [PubMed: 12052904]

Rzadzinska A, Schneider M, Noben-Trauth K, Bartles JR, Kachar B. Balanced levels of Espin are critical for stereociliary growth and length maintenance. Cell Motil. Cytoskel 2005;62:157–165.

Schöck F, Perrimon N. Molecular mechanisms of epithelial morphogenesis. Annu. Rev. Cell Dev. Biol 2002;18:463–493. [PubMed: 12142280]

Sekerková G, Loomis PA, Changyaleket B, Zheng L, Eytan R, Chen B, Mugnaini E, Bartles JR. Novel espin actin-bundling proteins are localized to Purkinje cell dendritic spines and bind the Src homology 3 adapter protein insulin receptor substrate p53. J. Neurosci 2003;23:1310–1319. [PubMed: 12598619]

Sekerková G, Zheng L, Loomis PA, Changyaleket B, Whitlon DS, Mugnaini E, Bartles JR. Espins are multifunctional actin cytoskeletal regulatory proteins in the microvilli of chemosensory and mechanosensory cells. J. Neurosci 2004;24:5445–5456. [PubMed: 15190118]

Sjöström B, Anniko M. Cochlear structure and function in a recessive type of genetically induced inner ear degeneration. ORL J. Otorhinolaryngol. Relat. Spec 1992a;54:220–228.

Sjöström B, Anniko M. Genetically induced inner ear degeneration. A structural and functional study. Acta Otolaryngol. Suppl. (Stockh.) 1992b;96:407–412.

Souter M, Nevill G, Forge A. Postnatal maturation of the organ of Corti in gerbils: morphology and physiological responses. J. Comp. Neurol 1997;386:635–651. [PubMed: 9378857]

Stone JS, Shang J-L, Tomarev S. Expression of Prox1 defines regions of the avian otocyst that give rise to sensory or neural cells. J. Comp. Neurol 2003;460:487–502. [PubMed: 12717709]

Tilney LG, Tilney MS, DeRosier DJ. Actin filaments, stereocilia and hair cells: how cells count and measure. Annu. Rev. Cell Biol 1992;8:257–274. [PubMed: 1476800]

Woods C, Montcouquiol M, Kelley MW. Math1 regulates development of the sensory epithelium in the mammalian cochlea. Nat. Neurosci 2004;7:1310–1318. [PubMed: 15543141]

Zheng JL, Gao W-Q. Analysis of rat vestibular hair cell development and regeneration using calretinin as an early marker. J. Neurosci 1997;17:8270–8282. [PubMed: 9334402]

Zheng L, Sekerková G, Vranich K, Tilney LG, Mugnaini E, Bartles JR. The deaf jerker mouse has a mutation in the gene encoding the espin actin-bundling proteins of hair cell stereocilia and lacks espins. Cell 2000;102:377–385. [PubMed: 10975527]

Zine A, Romand R. Development of the auditory receptors of the rat: a SEM study. Brain Res 1996;721:49–58. [PubMed: 8793083]

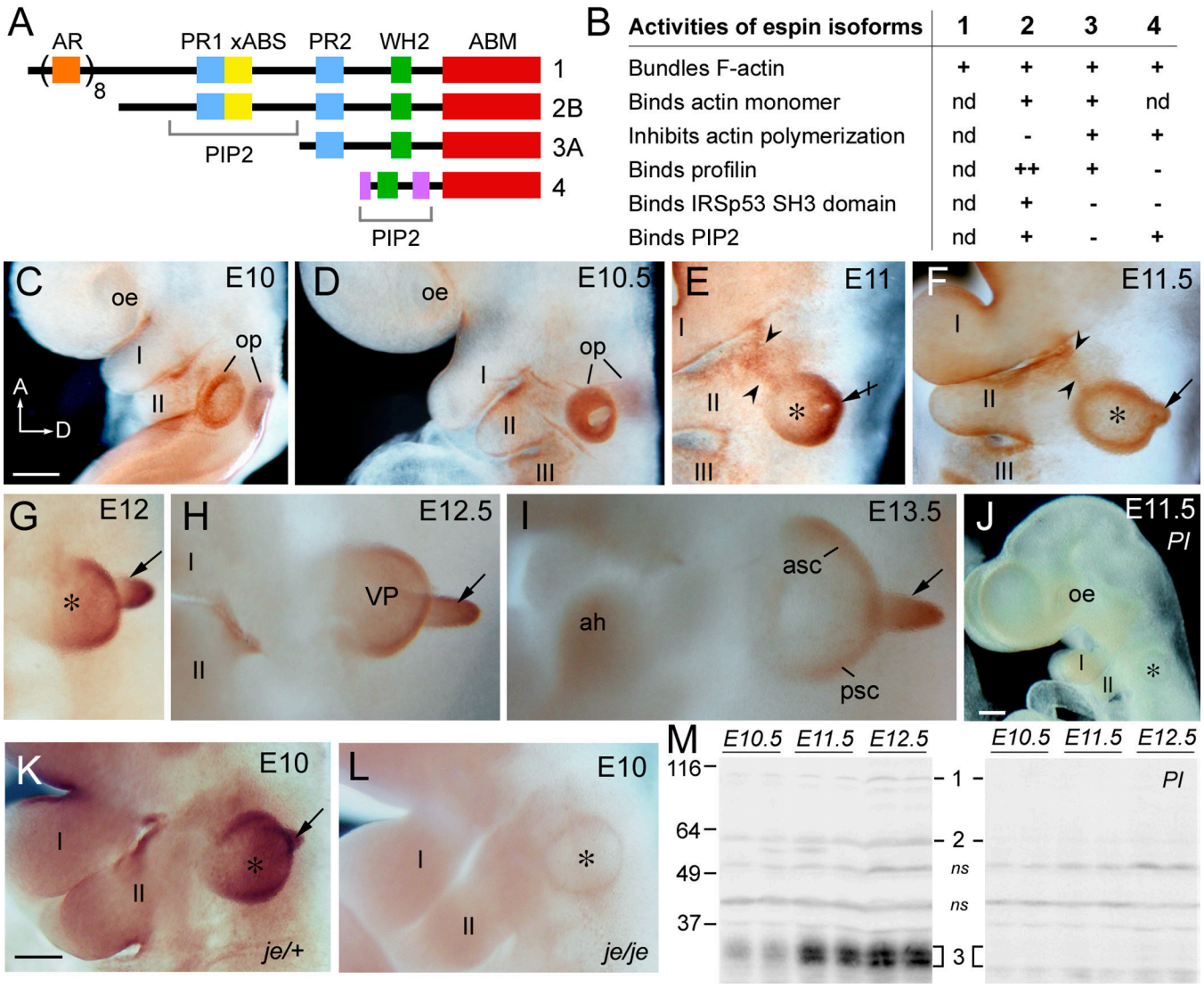

Fig.1. Espins isoforms in early inner ear development

(A) Stick-figure comparison of representative examples from each of the four major espin isoform size classes, highlighting known structural and functional domains. ABM, actin-bundling module; xABS, additional F-actin-binding site; AR, ankyrin-like repeat; PIP2, peptide regions required for binding phosphatidylinositol 4,5-bisphospate; PR1 and PR2, proline-rich peptide 1 and 2; WH2, Wiskott-Aldrich Syndrome protein homology 2 domain; purple, peptides encoded by exons that are unique to espin 4 (both are required for maximum PIP2 binding). (B) Summary of biological activities and ligand-binding sites for the four major size classes of espin isoform (for additional details, see Sekerková et al., 2003; 2004). nd, not determined. (C–L) Immunoperoxidase labeling of embryo whole-mounts with affinity purified pan-espin antibody shows strong, specific staining in the otic pit (op), the otocyst (asterisk), the developing membranous labyrinth – including endolymphatic duct (arrow), vertical canal pouch (VP), anterior semicircular canal (asc) and posterior semicircular canal (psc) – and the clefts between branchial arches (I, II, III). This staining is also observed in heterozygous jerker mouse embryos (K), but not in espin-deficient homozygous jerker mouse embryos (L) (E10 mouse, comparable to E11.5 rat), and is not observed with preimmune IgG (J). A, anterior; arrowheads, espin-positive region near

the acousticofacial preganglion complex (AFG) (see Fig. 2); ah, auditory hillock region; crossed arrow, otic pit closure; D, dorsal; oe, optic eminence. (M) Western blots of rat embryos labeled with affinity purified pan-espin antibody (left panel) or preimmune IgG (*PI*) (right panel) showing the presence of espin 3 isoforms (multiple bands at ~32–35 kDa; 3), and lower levels of espin 2 (~60 kDa; 2) and espin 1 (~110 kDa; 1). Duplicate lanes are shown. ns, nonspecifically labeled bands also detected using preimmune IgG; numbers at left, molecular mass in kDa. Scale bars, 200 μm in C–I,K,L; 500 μm in J.

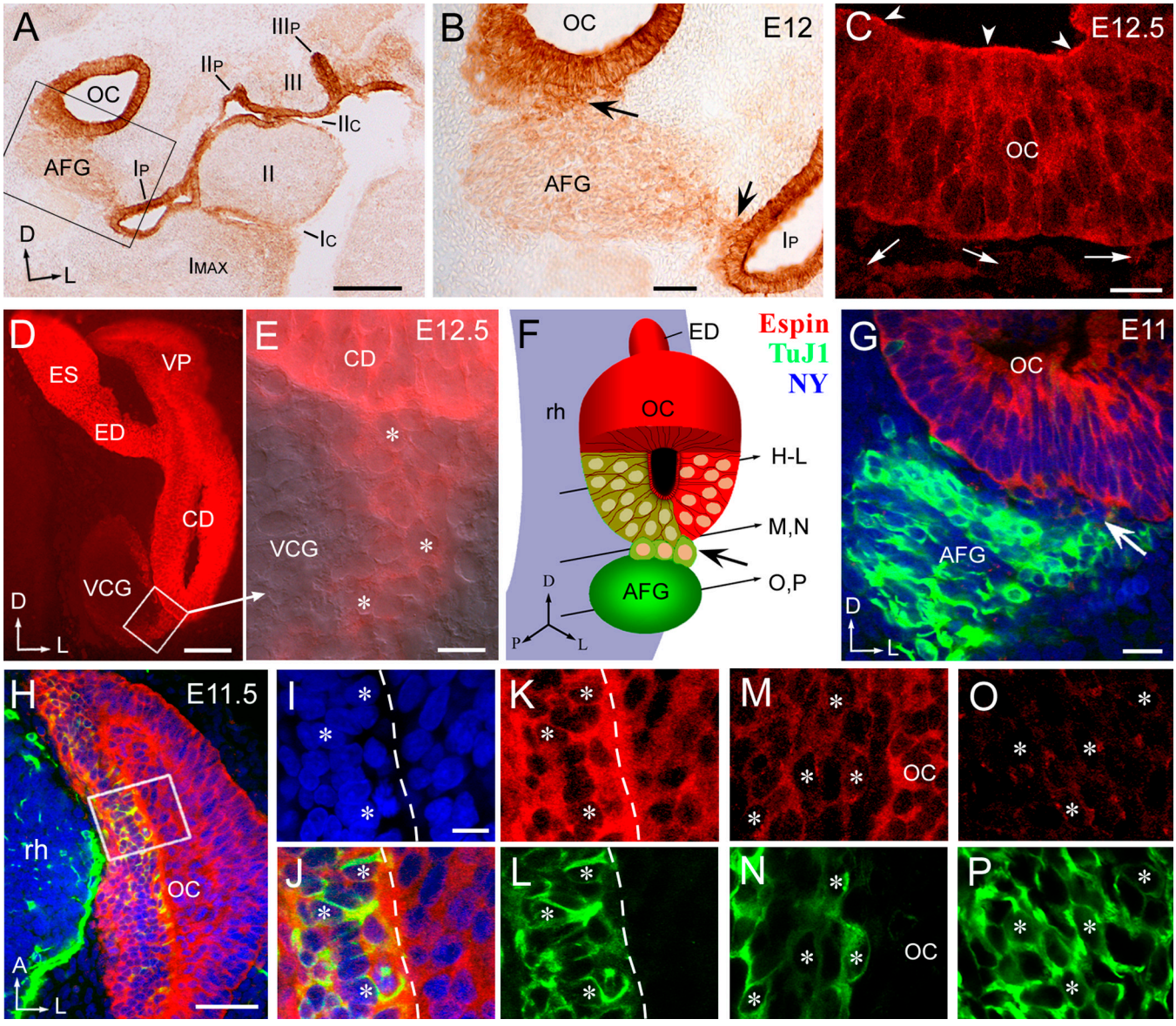

Fig. 2. Espins in otic, branchial-cleft and pharyngeal-pouch epithelia and delaminating neuroblasts

Axes show dorsal (D), lateral (L), anterior (A) and posterior (P) directions for these sections. (A–B) Espin immunoperoxidase labeling is present in the epithelium of the otocyst (OC), pharyngeal pouches (I_P–III_p) and branchial clefts (I_c, II_c). The acousticofacial preganglion complex (AFG) shows much lower labeling. B is the enlargement of the boxed area in A. Note cells of intermediate staining intensity at the AFG-otocyst and AFG-pharyngeal pouch borders (arrows in B). I_{max}, maxillary division of branchial arch I; II, III, branchial arches II and III. (C) In confocal sections, espin immunofluorescence is present throughout the cytoplasm of otic epithelial cells and enriched at the apical microvillar region (arrowheads). arrows, delaminated cells with moderate espin antibody labeling (see more below). (D,E) In embryo sections, espin immunofluorescence is distributed throughout the epithelium of the cochlear duct (CD), vertical canal pouch (VP), endolymphatic duct (ED) and endolymphatic sac (ES). The vestibulocochlear ganglion (VCG) shows moderate espin immunostaining at its periphery, especially near the cochlear duct (asterisks in E). E is the enlargement of the

boxed area in D with phase contrast added. (F) Schematic diagram of an otocyst with neuroblasts delaminating into the AFG (reference for G–P). Red, green and mustard colors depict areas labeled by espin antibody, class III β-tubulin (TuJ1) antibody, and both antibodies, respectively. Delaminating neuroblasts (arrow) are light green. NY, nuclear yellow (blue in G–J); ED, endolymphatic duct; rh, rhombencephalon. (G–P) Double-labeling of embryo sections with antibodies to espin (red) and TuJ1 (green) reveals the presence of espin in neuroblasts and its down-regulation upon delamination. (G) With standard fixation, the TuJ1 antibody intensely labels the cells in AFG, while the delaminating cells (arrow) are labeled only weakly. TuJ1 labeling in the otic epithelium is so weak that it is not readily discerned in this multicolor image. (H–P) When fixed approximately one-half as long, the TuJ1 antibody labels neuroblasts in the medial face of the otic epithelium adjacent to the rhombencephalon (rh) (H,J,L), delaminating neuroblasts (N) and cells of the AFG (P). I–L show enlargements of the box in H. The dashed line in I-L divides the otic epithelium into its medial and lateral faces. H–P are taken from different levels of the same embryo as shown in F. Note the graded decrease in espin immunofluorescence in the TuJ1-positive cells from otocyst (asterisks in K) to delaminating cells (asterisks in M) to cells of the AFG (asterisks in P). Scale bars, 200 μm in A; 50 μm in B,H; 20 μm in C,E,G; 100 μm in D; 10 μm in I–P.

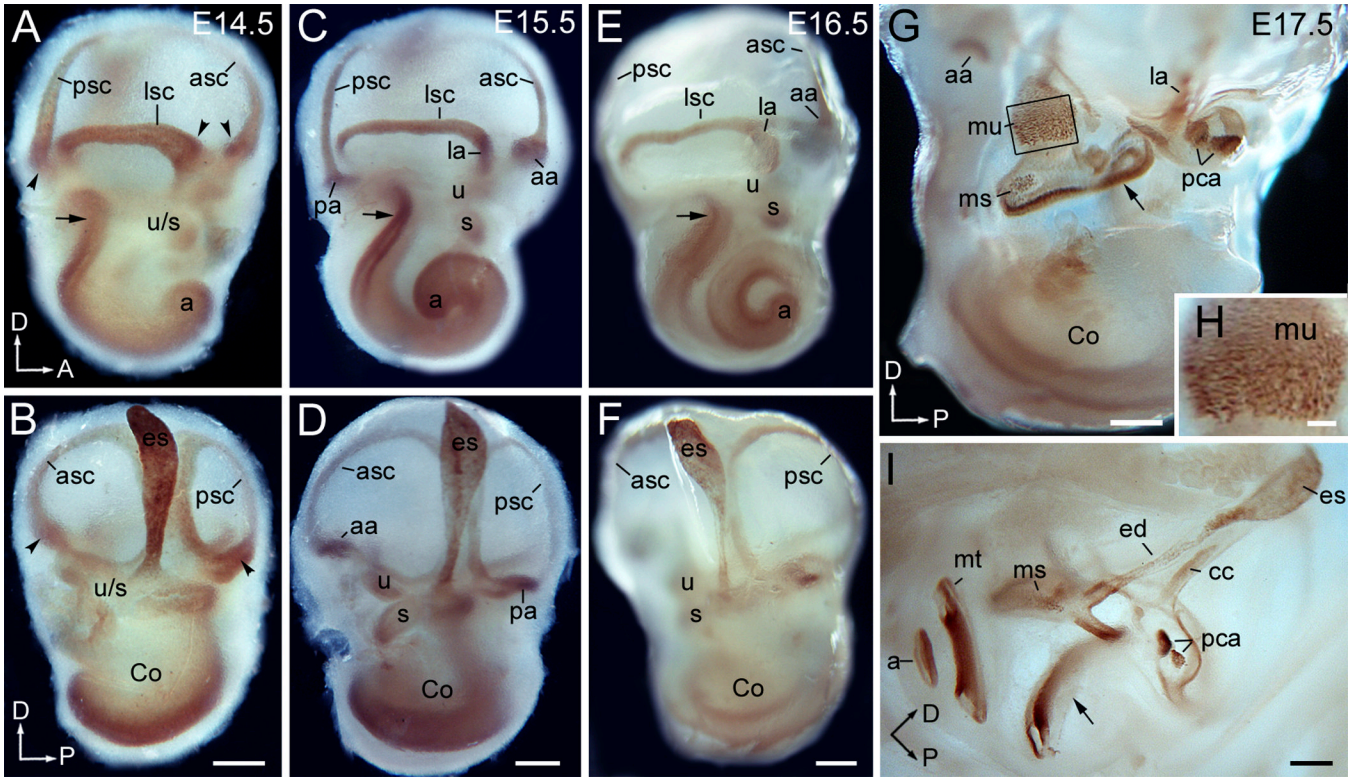

Fig.3. Espins in the developing membranous labyrinth

(A–F) Espin immunoperoxidase labeling is present throughout the epithelium of the membranous labyrinth in inner ear whole-mounts at E14.5 and E15.5. This general staining declines and becomes increasingly regionalized at E16.5 and beyond. (G,I) Espin immunoperoxidase labeling after partial removal of the capsule confirms the trend toward increasing regionalization within the labyrinth epithelium and reveals the labeling of HCs in the vestibular system. The latter are seen to best advantage as brown speckles in the macula ultriculus (mu) and macula sacculus (ms) in G and H. H is an enlarged image from the boxed area in G. a, apex of the cochlea; A, anterior; arrows, base of the cochlea; arrowheads, developing cristae ampullares in A and B; aa, anterior ampulla; asc anterior semicircular canal; cc, common crus; Co, cochlea; D, dorsal; es, endolymphatic duct; es, endolymphatic sac; la, lateral ampulla; lsc, lateral semicircular canal; mt, mid turn; P, posterior; pa, posterior ampulla; pca, posterior crista ampullaris; psc, posterior semicircular canal; u, utricule; s, saccule. Scale bars, 250 μm in A–G,I; 50 μm in H.

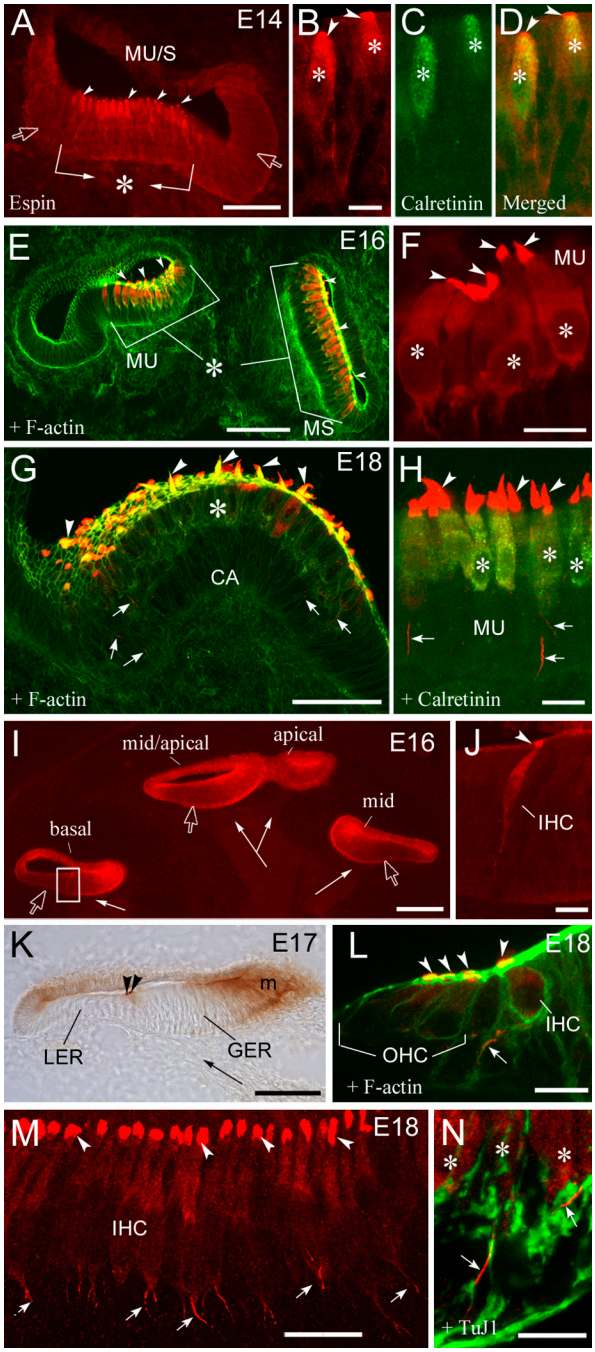

Fig.4. Espins during HC differentiation and stereociliogenesis

(A–M) Espin antibody-positive vestibular HCs (asterisks) are first recognized at E14 (A–D) in the ultriculosaccular region (MU/S) and are surrounded by epithelial cells showing decreased general cytoplasmic immunostaining (opened arrows). Calretinin antibody labeling (green in C,D,H) is used as a vestibular HC marker. Espin antibody-positive cochlear IHCs and OHCs appear later, at E16 (I,J) and E18 (L), respectively. J is the enlargement of the boxed area in I. The general cytoplasmic immunostaining is decreased in the epithelial cells in the expected HC region of the cochlea (open arrows in I). Immunoperoxidase labeling (K) shows that this zone of decreased staining grows to encompass the lesser epithelial ridge (LER) and much of the adjoining greater epithelial

ridge (GER), causing the cytoplasmic immunostaining to become increasingly enriched in the epithelial cells of the modiolar face (m). In HCs espins are enriched at the apex, in the developing stereocilia (arrowheads), but are also detected in the apical cytoplasm. Note, that the cytoplasmic labeling of early vestibular HCs (A,B) appears stronger than that of early cochlear HCs (J). The level of espin immunofluorescence in HCs and its extent of compartmentalization to stereocilia (arrowheads) increase during HC differentiation in the vestibular system (E–H) and cochlea (L,M). Accordingly, espin is increasingly colocalized with the stereociliary F-actin as revealed by fluorescent-phalloidin (green in E,G). Intense labeling for F-actin with fluorescent phalloidin all along the luminal surface of Kölliker's organ at this stage (green in L) was noted previously (Romand et al., 1993). arrows, espin-rich basal processes (see below); CA, crista ampullaris; long arrows in I,K, trajectory of nerve tracks; MS, macula sacculus; MU, macula utriculus. (G,H,L–N) At E18 espin immunofluorescence is also present in a peculiar tail-like process (arrows) that emanates from the base of cochlear IHCs (L,M) and vestibular HCs (H,N). These processes are also evident in G in the HCs at the edges of a crista ampullaris, but are difficult to see without increasing magnification. The espin-positive basal processes are distinct from nerve processes as revealed by double-labeling with TuJ1 antibody (green in N). Scale bars, 50 μm in A,G,K; 10 μm in B–D,F,H,J,L,M; 100 μm in E,I; 5 μm in N.

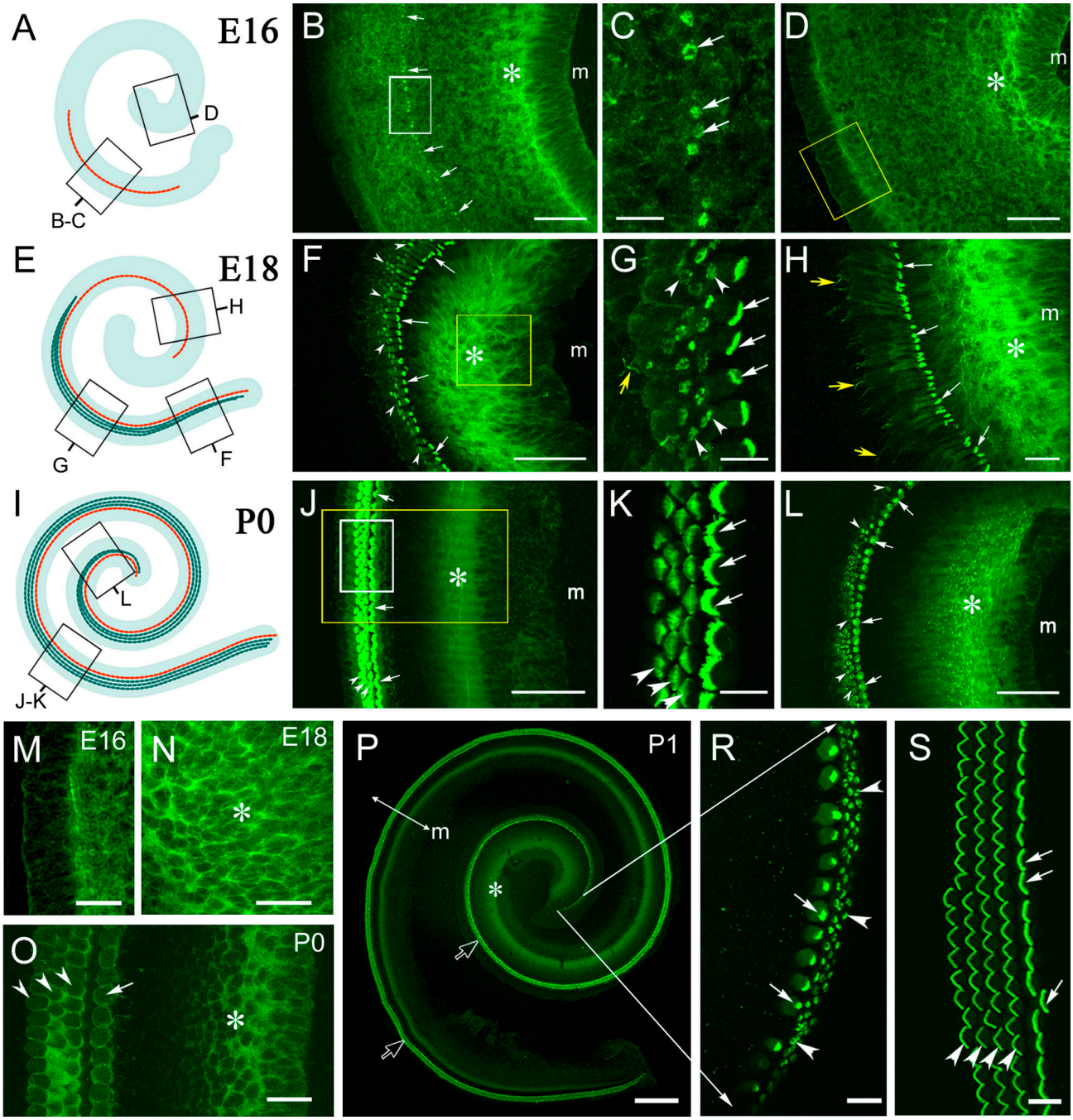

Fig.5. Cochlear espins in late embryos and neonates

(A–P) In cochlear surface preparations, the espin immunostaining initially observed throughout the entire cochlear epithelium progressively decreases and becomes regionalized to epithelial cells (asterisks) at the modiolar face (m) as HCs appear – IHCs (arrows) first, followed by OHCs (arrowheads) – and become aligned in rows in a gradient from base to apex along the cochlear spiral. In the diagrams in A,E,I, red depicts IHCs, and green depicts OHCs. C and K are enlargements of white boxes in B and J, respectively, showing accumulation of espin in developing HC stereociliary bundles. Examination of the cut face in M, which is the enlargement of the yellow box in D, confirms a decrease in cytoplasmic espin immunostaining concurrent with a retention of some immunostaining at the apical

surface at E16 (see Fig. 4I,J). N and O are confocal sections from a deeper plane through the areas in the yellow boxes in F and J, respectively, to reveal cytoplasmic immunostaining. P shows the entire cochlear spiral at P1. Note the closely spaced rows of HCs (spiral band marked with open arrows) and decreasing apex-to-base gradient in general immunostaining of epithelial cells in the modiolar region (spiral band marked by asterisk at apex). yellow arrows, espin-rich basal processes. (R,S) At P1, HCs at the extreme apex are in an immature state of differentiation (R), while unaligned or supernumerary HCs with espin-positive stereocilary bundles (S) are present in the middle turn. Scale bars, 50 μm in B,D,F,J,L; 10 μm in C,G,K,R,S; 20 μm in H,M–O; 200 μm in P.

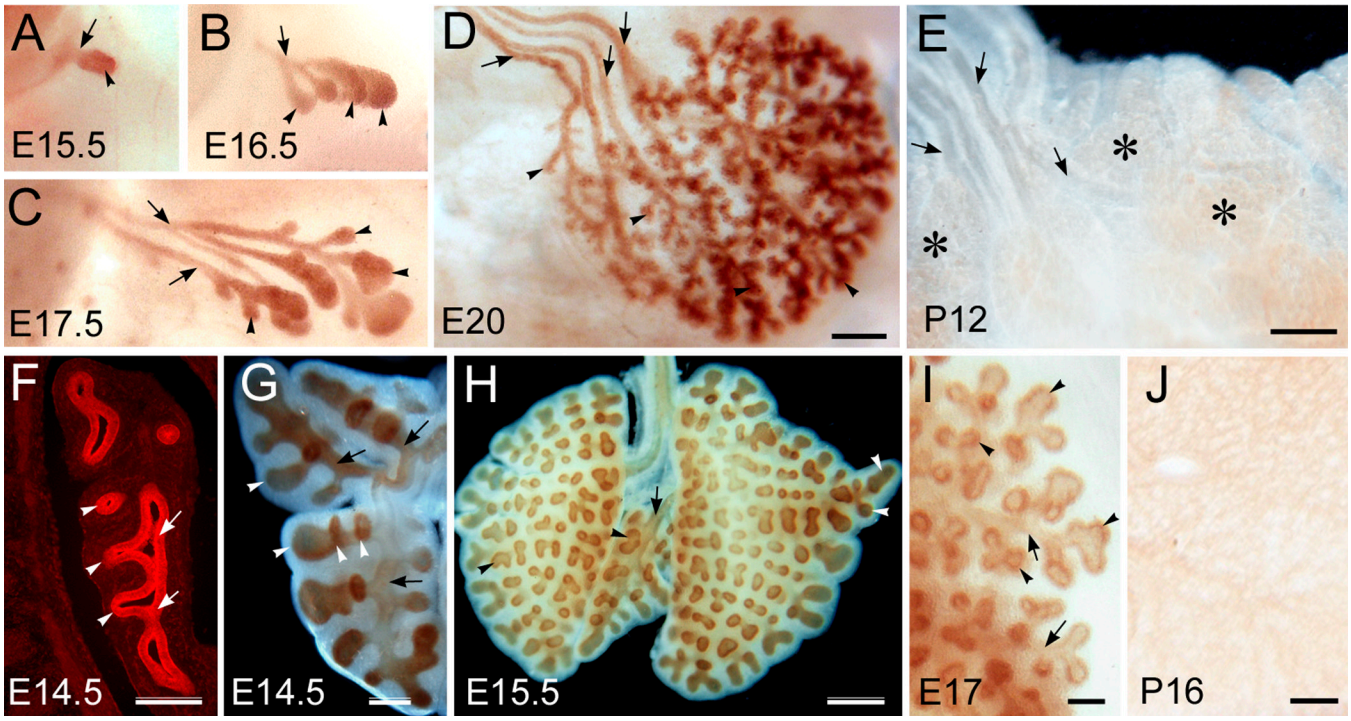

Fig.6. Espins during epithelial branching morphogenesis in lacrimal gland and lung

(A–D, G–I) Developing lacrimal gland in embryo whole-mounts (A–D, same magnification) and whole-mounts of developing lung (G–I) show intense espin immunoperoxidase labeling in the epithelium of ducts (arrows) and buds (arrowheads) from early stages through periods of extensive branching morphogenesis. At E17 in the lung, the buds, especially their distal portions, appear to be more intensely labeled than ducts (I). (F) Immunofluorescence of lung section confirms that the espin is distributed throughout the epithelium of ducts (arrows) and buds (arrowheads). (E,J) The level of immunostaining is dramatically reduced by P12 in lacrimal gland (E, whole-mount) and by P16 in lung (J, ~1 mm-thick tissue slab). Scale bars, 250 μm in A–G,J; 500 μm in H; 100 μm in I.

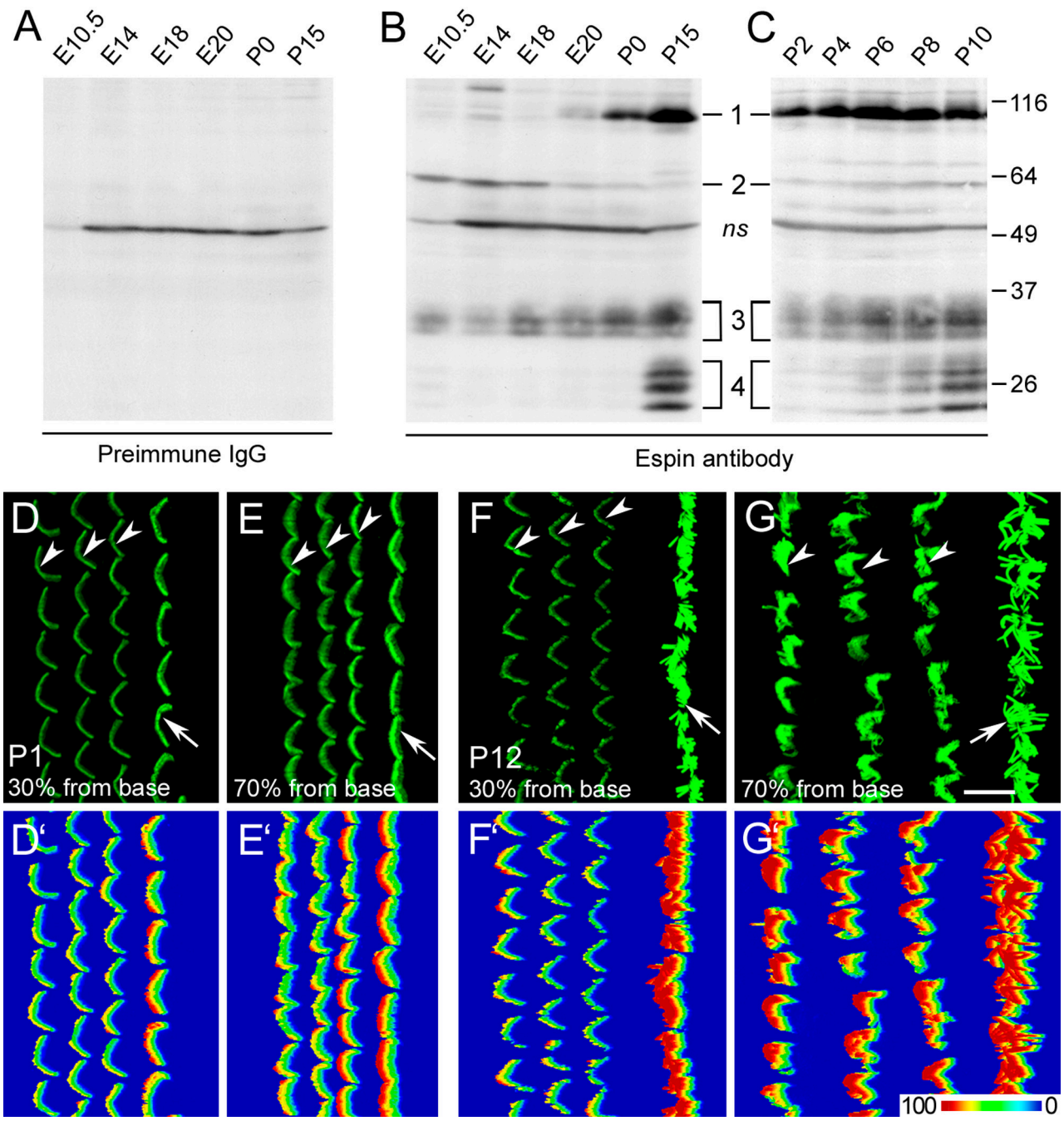

Fig.7. Espins isoforms in inner ear during embryonic development and postnatal maturation

(A–C) Western blots of inner ear-enriched specimens labeled with pan-espin antibody (B,C) or preimmune IgG (A) showing the following major trends: the retention and gradual increase in espin 3 isoforms (multiple bands at ~32–35 kDa; 3), the decrease in espin 2 (~60 kDa; 2) after E18, the increase in espin 1 (~110 kDa; 1) beginning at E20 and continuing during the first days of postnatal life, and the increase in espin 4 isoforms (multiple bands at ~22–28 kDa; 4) from P6 through P10. SDS extracts prepared from specimens containing approximately equal masses of wet tissue derived from anterior embryo halves (E10.5), inner ear regions (E14) or bony labyrinths (E18 onward). ns, nonspecifically labeled bands also detected using preimmune IgG; numbers at right, molecular mass in kDa. (D–G)

Immunofluorescence of cochlear surface preparations comparing espin levels at P1 (D,E) and P12 (F,G) in HCs positioned ~30% (D,F) and ~70% (E,G) from the base along the cochlear spiral, showing correlation between increases in espin levels and postnatal stereocilium elongation. At P1, espin levels increase only slightly from the ~30% position to the ~70% position (D,E), whereas, at P12, espin levels increase more dramatically from the ~30% position to the ~70% position (F,G). This is especially noticeable for OHCs (arrowheads). The increase in IHCs (arrows) between the ~30% and ~70% positions at P12 (F,G) cannot be discerned because at this exposure the IHC signals are over-saturated. Note also a significant difference in espin levels between inner and OHCs, especially at the 30% position at P12 (D'–G'). Color-scale representation of espin immunofluorescence levels. arrows, IHCs. Scale bar,10 μm.